

Submillimetre Variability of Eta Carinae: cool dust within the outer ejecta

H.L. Gomez^{1*}, C. Vlahakis², C.M. Stretch¹, L. Dunne³, S.A. Eales¹, A. Beelen⁴,
E.L. Gomez^{5,1}, M.G. Edmunds¹

¹ School of Physics & Astronomy, Cardiff University, The Parade, Cardiff CF24 3AA, UK

² Leiden Observatory, Leiden University, PO Box 9513, 2300 RA Leiden, The Netherlands

³ School of Physics & Astronomy, University of Nottingham, University Park, Nottingham, NG7 2RD, UK

⁴ Institut d'Astrophysique Spatiale, bât 121, Université Paris-Sud, 91405, Orsay, Cedex, France

⁵ Las Cumbres Observatory Global Telescope Network, Inc., 6740 Cortona Dr, Suite 102, Goleta, CA 93117, USA

7 November 2018

ABSTRACT

Previous submillimetre (submm) observations detected $0.7 M_{\odot}$ of cool dust emission around the Luminous Blue Variable (LBV) star η Carinae. These observations were hindered by the low declination of η Carinae and contamination from free-free emission originating from the stellar wind. Here, we present deep submm observations with LABOCA at $870 \mu\text{m}$, taken shortly after a maximum in the 5.5-yr radio cycle. We find a significant difference in the submm flux measured here compared with the previous measurement: the first indication of variability at submm wavelengths. A comparison of the submm structures with ionised emission features suggests the $870 \mu\text{m}$ is dominated by emission from the ionised wind and not thermal emission from dust. We estimate $0.4 \pm 0.1 M_{\odot}$ of dust surrounding η Carinae. The spatial distribution of the submm emission limits the mass loss to within the last thousand years, and is associated with mass ejected during the great eruptions and the pre-outburst LBV wind phase; we estimate that η Carinae has ejected $> 40 M_{\odot}$ of gas within this timescale.

Key words: submillimetre - stars: individual (η Carinae): mass loss - dust

1 INTRODUCTION

η Carinae (η Car), one of the most luminous infra-red (IR) objects in our Galaxy ($>10^6 L_{\odot}$), is well known for dramatic outbursts over the last thousands of years, in which vast amounts of material is ejected outwards from the star. The great eruption phase during the last 200 years are responsible for creating the dusty bipolar nebula known as the Homunculus, as seen in the *Hubble Space Telescope* (*HST*) images. The recent discovery of a fast blast wave from the 1843 eruption (Smith 2008) indicates that the mass loss in η Car is not simply due to a stellar wind, but could be more akin to a low-energy supernova remnant. Extensive IR imaging has revealed important clues about the mass loss history; the Infrared Space Observatory (ISO) discovered a massive cool dust component (Morris et al. 1999; Smith et al. 2003) with a total of $\sim 0.1 M_{\odot}$ of dust proposed to be present in the nebula, suggesting a mass loss rate of $0.5 M_{\odot} \text{ yr}^{-1}$ during the last 200 years. Submillimetre (submm) observations (Gomez et al. 2006, hereafter G06) of η Car at 450 and $850 \mu\text{m}$ with the Submillimetre Common User Bolometer Array (SCUBA) detected the presence of a massive component of dust, with $\sim 0.7 M_{\odot}$ needed to reproduce the IR-submm Spectral En-

ergy Distribution (SED). Their work suggested that up to four times more mass had been ejected from η Car during its recent, violent history than previously proposed. The SCUBA data also indicated that the cool dust component was extended along the mid-plane, far beyond the inner optical and IR region; this was interpreted as mass which had been ejected on a much longer timescale than the well-known, smaller features such as the torus and Homunculus.

The previous analysis of the SCUBA data was hindered by two unknowns: whether the submm emission originated from free-free and not thermal emission from dust and whether the extended structure was reliable. Firstly, the submm fluxes are likely to be contaminated by strong free-free emission from the extended stellar wind which is thought to vary with frequency as $\nu^{0.6-1.3}$ (e.g. Cox et al. 1995; Brooks et al. 2005, hereafter B05). This is further compounded since the radio and millimetre (mm) fluxes are highly variable, with η Car at 3 cm changing appearance from a point source in 1992 to an extended region with five times more flux in 1996 (Duncan & White 2003). The X-ray, radio and mm variability of η Car has been well documented (Pittard et al. 1998; Abraham et al. 2005; Damineli et al. 2008), with the star undergoing periodic variability over a 5.5-yr period. This variability has been associated with shocks from an extended disc surrounding the η Car binary system (e.g. Duncan & White 2003) and/or due to episodic mass loss which, in turn, decreases the number of ionising

* E-mail: haley.gomez@astro.cf.ac.uk

photons. Since there were no available mm observations to match the epoch of the original 1998 SCUBA data (taken during the minimum phase of the radio cycle), G06 were not able to estimate the contribution to the submm due to free-free emission. Second, the SCUBA data were taken at very large airmass ($A \sim 5.5$) due to the declination of η Car. This meant that the beam shape at $450 \mu\text{m}$ was distorted due to the deformation of the dish at such low elevations and the morphology of the source was difficult to ascertain from this dataset. Accurately determining the distribution and mass of dust in the stellar wind has enormous consequences not only on determining the mass loss history of η Car, but also understanding the progenitors of ‘exotic’ core-collapse supernovae (SNe; Pastorello et al. 2007; Smith et al. 2009).

In this Letter, we present deep submm LABoCa observations of η Car, taken shortly after the maximum phase in the cycle. In §2 we discuss the data reduction and compare the $870 \mu\text{m}$ emission to well-known features seen in X-ray, optical, $\text{H}\alpha$, $8 \mu\text{m}$ and 1.2mm in §3. In §4 we estimate the dust and gas mass for the stellar wind and our conclusions are presented in §5.

2 OBSERVATIONS AND DATA REDUCTION

The $870 \mu\text{m}$ data were taken with the LABoCa camera (Siringo et al. 2009), a 295-pixel bolometer array, located on the Atacama Pathfinder EXperiment telescope (Güsten et al. 2006) on Chanjantor in Chile. η Car was observed during Science Verification on 23rd July 2007. This epoch corresponds to 1.4 yrs after maximum brightness in the radio and X-ray cycles (2006.25). The observations were carried out in raster spiral mode with twelve scans, each providing a fully sampled map over $30' \times 30'$. The total on-source integration time was 1.7 hours. Two independent measurements of the optical depth, τ were obtained. The first method used the precipitable water vapour (PWV) levels measured every minute along the line of sight, then scaled using the relevant atmospheric transmission model. The PWV ranged from 0.7–0.9 mm. The second method calculated τ from skydip measurements, where a model of the dependence of the effective sky temperature on elevation were fitted to determine the zenith opacity. The two skydips taken before and after the on-source scans were both well fitted by the model, with τ between 0.1–0.2. These values were 25% lower than those estimated from the PWV measurements. A linear combination of the two methods, and a final comparison with the calibrator models (e.g. Siringo et al. 2009), was used to determine the values used in the data reduction. Following Dunne & Eales (2001), the fractional error in the flux from the error due to the range of opacities calculated with these two methods is 6 per cent.

The data were reduced using the BoA (BOLometer array Analysis software) package. The focus was checked on observations of Venus and Jupiter and was stable within $\pm 0.2 \text{mm}$. Pointing observations were within $1''$ in azimuth and elevation during the earlier scans but crept up to within $3''$ towards the end. Bad and noisy pixels were flagged, with 276 bolometers used in each scan. The data were despiked and correlated noise was removed. The reduction is optimized for the recovery of strong sources. The scans were coadded (weighted by rms^{-2}) and the data were gridded onto $6''$ pixels to create the final map. After a first iteration of the reduction, the source map was used to flag bright sources and the data were reduced again. This was efficient at removing negative artifacts which appear around the bright sources in the first iteration and led to a more stable background noise level in the central region ($\sim 40 \text{mJy beam}^{-1}$). The $870 \mu\text{m}$ map towards η Car is shown

in Fig. 1 together with $8 \mu\text{m}$ *Midcourse Space eXperiment (MSX)* archival data. η Car is the strongest source in the LABoCa map, and peaks at signal-to-noise > 100 . Well known emission regions, molecular clouds and star clusters are identified in the image.

Secondary calibrators were used to calibrate the map and the typical correction factor when comparing the measured flux on the calibrator with its expected flux in an aperture was ~ 5 per cent. The total uncertainty in the calibration, including uncertainties in the calibrator model is therefore ~ 12 per cent. The $870 \mu\text{m}$ flux of η Car measured in an aperture with radius $30''$ is $42 \pm 5 \text{Jy}$, compared to the flux estimated by SCUBA in 1998 of $13 \pm 1 \text{Jy}$ (G06). This is an increase by a factor of three over the 9 yr period and cannot be accounted for by calibration errors.

3 RESULTS

A zoomed in image of η Car is presented in Fig. 1 and compared with $\text{H}\alpha$ (Smith, Bally & Morse. 2003) and 1.2mm (B05) emission. Faint structures not previously seen in FIR-submm maps are detected with LABoCa and are identified with well known sources (labeled in Fig. 1 following the notation of Smith et al. 2003 & B05). The submm emission can be separated into four components: the bright source at the location of η Car; filaments and arcs which surround molecular globules (Rathborne et al. 2002); peaks and filaments associated with molecular clouds at the edges of the map; and a number of compact sources (seen at mm and submm wavelengths, but not always in $\text{H}\alpha$ and $8 \mu\text{m}$). The edges of the two large molecular clouds, part of a giant cloud complex within the Carina arm, are visible in the LABoCa map to the North and South of η Car. The $870 \mu\text{m}$ flux in these regions correlates with peaks seen in molecular emission (Cox et al. 1995; Yonekura et al. 2005) suggesting dust emission from cold clouds.

η Car is the brightest source at $870 \mu\text{m}$ and 1.2mm , but not at IR-FIR. At 12 and $25 \mu\text{m}$, the peak is found at the centre of Tr 14 (a massive star cluster) whereas at 60 and $100 \mu\text{m}$, the peak shifts towards the west (and the Car I feature). This shift traces a temperature gradient in the nebula (Cox 1995); hotter dust is located closer to Tr 14, where massive stars are externally heating the clouds and cooler material is forced further away. The shift in peak emission from IR-FIR is also seen in our submm data.

The faint structure just north of η Car is associated with the Car II emission feature. The $870 \mu\text{m}$ emission closely follows the $\text{H}\alpha$, $8 \mu\text{m}$ and 1.2mm emission (Fig. 2) and at longer wavelengths, the 3cm radio emission (B05). These arcs and filaments surround dark clouds detected in CO emission (Rathborne et al. 2002, Cox & Bronfman 1995). The close correlation between ionised gas, emission at both mm and radio wavelengths and the LABoCa emission suggest that the $870 \mu\text{m}$ originates from ionised material. Indeed, the integrated flux of Car II at $870 \mu\text{m}$ here agrees with the extrapolated radio continuum spectrum in B05 (their Fig 5) which are well fitted with an HII emission model. The ratio of the $870 \mu\text{m}/1.2 \text{mm}$ maps confirm that the spectral index in Car II varies as $F_\nu \propto \nu^{-2}$, consistent with an ionization front or HII region, thus the LABoCa emission here originates from a free-free source and not from warm dust. Our lack of submm detection at the location of the famous Keyhole Nebula (labeled 1-3, Fig. 1) rules out any dust component with temperatures higher than 13K .

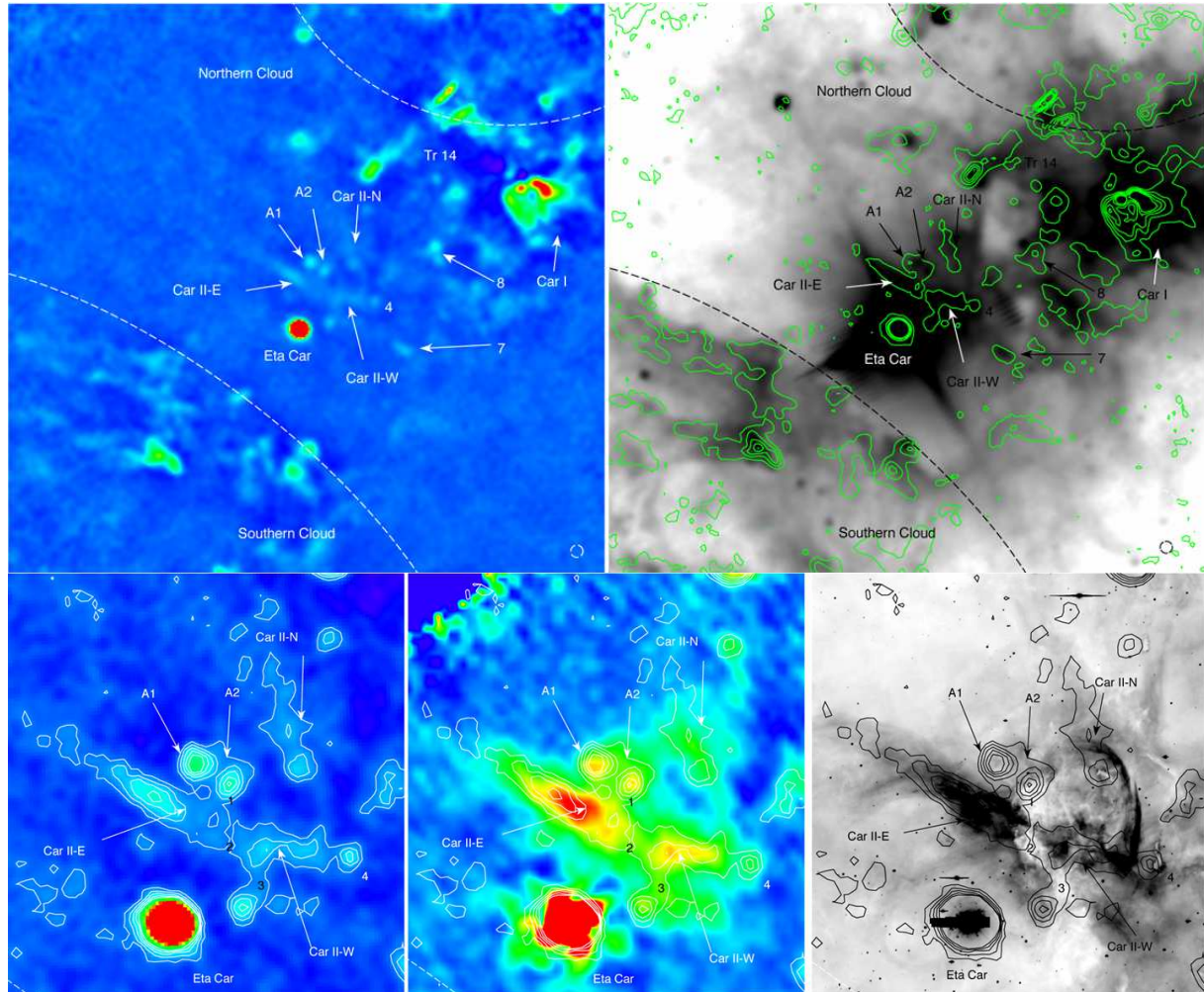


Figure 1. The environment surrounding η Car. **Top Panel:** *Left:* LABoCa $870\ \mu\text{m}$ emission. *Right:* MSX $8\ \mu\text{m}$ emission, shown here in negative log greyscale, with LABoCa $870\ \mu\text{m}$ contours (starting at $0.04\ \text{Jy beam}^{-1}$). Region shown covers $19' \times 19'$ area with LABoCa beam size shown in lower right hand side. Known compact sources are labeled 4-8 (B05). **Bottom Panel:** Zoomed in region ($9' \times 8.4'$) with LABoCa $870\ \mu\text{m}$ contours overlaid, ranging from 0.04 – $0.25\ \text{Jy beam}^{-1}$. *Left:* LABoCa emission. *Middle:* $1.2\ \text{mm}$ emission (SIMBA map kindly provided by K Brooks B05). *Right:* $H\alpha$ emission shown here in negative greyscale (CTIO map kindly provided by N Smith, Smith, Bally & Morse 2003). The Keyhole Nebula is labeled 1, 2 and 3.

3.1 Submillimetre Emission from η Carinae

The central η car source as seen with LABoCa (Figs. 1 & 2) is well fitted by a two-dimensional Gaussian with FWHM $22''$. We find that η car is unresolved with the LABoCa beam ($19''$) and we see the first error beam pattern below 1 per cent peak intensity at $0.3\ \text{Jy beam}^{-1}$. Deconvolving from the beam and pixel size indicates a central source with FWHM $\sim 10''$. We do not detect the structure along the midplane seen in the original $850\ \mu\text{m}$ data from G06, confirming the suggestion made there that a combination of high airmass and chop throw had smeared the signal across the mid-plane. Based on the LABoCa observations, the true extent of the submm source is likely to be within the Homunculus ($18''$) and interior to the region encompassed by the O III ‘cocoon’ of material ($60''$) detected by Smith, Morse & Bally (2005). Recently, Smith (2008) detected a fast blast wave, traveling at up to $6000\ \text{km s}^{-1}$, from the great eruption in 1843. This blast wave extends out to the same radius as the cocoon, and is interior to or coincident with, the X-ray emission. Smith proposed that the X-rays arise from this fast blast wave running into a previous eruption which gave rise to a nitrogen rich shell. Such a scenario places severe constraints on

the timescales for emission seen interior to the blast wave material and suggests that the source responsible for the emission seen by LABoCa was ejected within the last 200–1000 years.

The $1.2\ \text{mm}$ emission from η Car is closely correlated with the $870\ \mu\text{m}$, and neither correlate well with the IR-FIR central source. If we assume that the former originates from thermal emission from dust grains (i.e. $F_\nu \propto \nu^{3+\beta}$), the ratio of $870\ \mu\text{m}/1.2\ \text{mm}$ would require a dust emissivity index, β , of -2 . If we assume emission at both wavelengths originates from a source which varies as $F_\nu \propto \nu^{-\alpha}$, we obtain $\alpha = 0.5$ – 2 which agrees well with emission from an ionised stellar wind source. The similar variability seen at both $870\ \mu\text{m}$ and $1.2\ \text{mm}$ suggests that less than 20 per cent of the $870\ \mu\text{m}$ flux is contributed by dust emission.

4 DISCUSSION

4.1 The Spectral Energy Distribution of η Car

The spectral energy distribution (SED) of η Car is shown in Fig. 3. Given the variability of observed fluxes over different epochs dur-

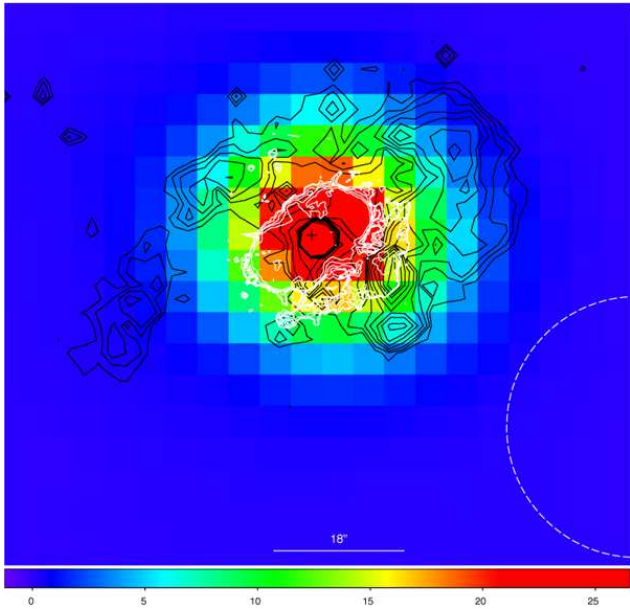


Figure 2. LABoCa 870 μm emission of η Car with archival X-ray (CHANDRA) and optical (*HST*) contours shown in black and white respectively. The LABoCa beam ($19''$) is shown in the lower right hand side. Units are Jy beam^{-1} . The extent of the Homunculus seen as the double-lobe structure in the contours is $\sim 18''$.

ing η Car’s radio cycle, we represent the variability as vertical bars following B05, highlighting the flux changes over the cycle rather than the fluxes measured at different epochs.

There are three major components to the SED: thermal emission from dust grains (following a modified blackbody with power-law index β), free-free emission from the ionised stellar wind and free-free emission from the optically thin Little Homunculus feature, seen close to the central star (Duncan & White 2003). The stellar wind material consists of two separate components: the optically thin varying as $\nu^{1.3}$ (e.g. B05) and the optically thick varying as a classical wind with $\nu^{0.6}$ (Wright & Barlow 1975; Lamers & Cassinelli 1999). The optically thin component from the Homunculus is produced by the ionisation of η Car’s stellar wind by the UV-radiation field of the hot binary companion. This produces free-free emission which varies as $\nu^{-0.1}$ and relates to the Little Homunculus and torus (Teodoro et al. 2008).

For the dust component, we used two-modified blackbodies:

$$S_\nu = N_h \nu^\beta B(\nu, T_h) + N_w \nu^\beta B(\nu, T_w) \quad (1)$$

where N is the normalisation term, β is the dust emissivity index and B is the Planck function at frequency ν and temperature T . The SCUBA 850 and LABoCa 870 μm fluxes are not included in the fit to the thermal emission from dust. The 450 μm was corrected for free-free emission expected at this wavelength using the predicted power-law variation $\nu^{0.6}$ (as shown in Fig. 3) where ~ 35 per cent of the 450 μm 1998 flux could originate from free-free emission. The revised 450 μm flux due to dust in the stellar wind is therefore $\sim 30 \text{ Jy}$. This agrees with the results from the Balloon-borne Large Aperture Submillimeter Telescope who observed η Car from 250–500 μm during the maximum in 2006 (Hargrave priv. comm., Hargrave et al. in prep). Hargrave et al. find no evidence of an increased flux at 500 μm when compared to the SCUBA 450 μm observed during the minimum. This supports the idea that the 450 μm flux measured with SCUBA is still dominated

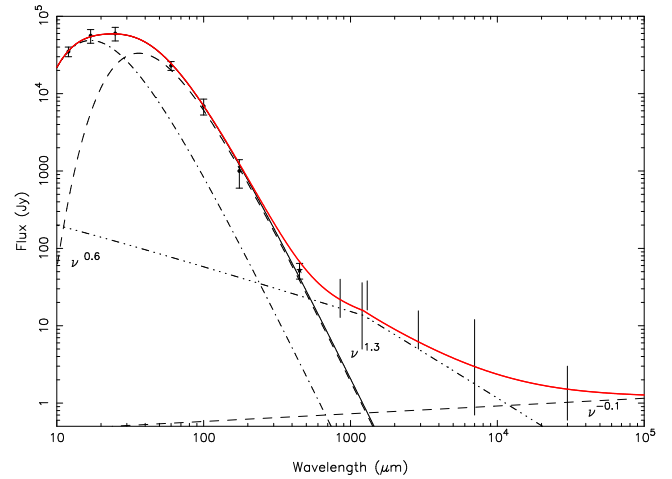


Figure 3. The SED of η Car from 12 μm through to the radio. The radio, mm and 850/870 μm fluxes are shown as vertical bars (following B05) to indicate their variability range during the 5.5-yr cycle. The solid black line is the sum of the two-temperature components fitted to the IR ($T_h = 174 \text{ K}$ and $T_w = 82 \text{ K}$) and 450 μm fluxes (dot-dashed and dashed respectively). The dot-dot-dot-dashed line shows the SED expected from the optically thick free-free wind, $F_\nu \propto \nu^{0.6}$ and the optically thin wind with $\propto \nu^{1.3}$. The dashed line represents emission from the optically thin Little Homunculus feature $\propto \nu^{-0.1}$. The red line shows the total SED from all the components. The far-IR luminosity from 12–1000 μm is $1.6 \times 10^6 L_\odot$.

by thermal emission from dust grains and does not undergo significant variability. Note that the 450 μm flux is key to the dust mass estimation since this extra constraint forces the fit to have a lower dust temperature and a steeper emissivity index than the previous published models (Morris et al. 1999; Smith et al. 2003; B05). We rule out a cold dust component since we cannot obtain a modified blackbody fit to the submm-mm fluxes. An adequate fit can be obtained using only the mm fluxes but this would require a dust component with $T \sim 4 \text{ K}$; it is difficult to understand how such cold dust could survive the close environment of η Car.

The dust mass is estimated using Eq. 2:

$$M_d = \frac{S_{450} d^2}{\kappa_{450}} \left(\frac{N_h}{B(\nu_{450}, T_h)} + \frac{N_w}{B(\nu_{450}, T_w)} \right) \quad (2)$$

where κ_ν is the dust-mass-absorption coefficient ($0.27 \text{ kg}^{-1} \text{ m}^2$ for interstellar dust at 450 μm , James et al. 2002) and d is the distance to the star. The best-fit (χ^2) to the SED requires a total dust mass of $0.4 \pm 0.1 M_\odot$ and $\beta \sim 1.9$ (indicative of normal interstellar dust grains), $T_h = 174_{-8}^{+16} \text{ K}$ and $T_w = 80_{-6}^{+10} \text{ K}$. The errors are estimated from the bootstrap technique where 1000 fits to the fluxes were made; the 68% confidence intervals are quoted here. Previous authors required $\beta \sim 1$ to fit the mid-IR SED but higher values are necessary to fit the long-wavelength submm fluxes at 450 and 870 μm .

The “transition” between the classical $\nu^{0.6}$ and $\nu^{1.3}$ power-law regimes from the stellar wind as plotted in Fig. 3 was noted in Cox et al. (1995) and B05 and is required to explain the observed SED at mm wavelengths. They proposed that this transition occurs due to changes in the ionisation properties of the wind but the location of this transition is not well constrained and consequently affects the amount of free-free emission expected at submm wavelengths. For example, if the two power-law regimes turned-over at 870 μm instead of 1.2 mm as plotted here, this would suggest that 100 per cent of the 870 μm flux and 65 per cent of the 450 μm could

originate from a free-free source. Changes to the wavelength of the transition will change the derived properties which fit the thermal dust SED (T , β) and the dust mass, but these changes are well within the errors quoted above. The exact location of this transition, though important to understand for physical reasons, does not affect the dust mass estimated in the current work.

With gas-to-dust ratio ~ 100 (Smith & Ferlund 2007), we estimate that $>40 M_{\odot}$ of gas has been ejected. This is approximately half of the value quoted in G06 but three times more than the maximum values quoted from previous IR data (Morris et al. 1999; Smith et al. 2003). Our estimate is also consistent with the upper end of the mass range (15–35 M_{\odot}) found by Smith & Ferlund (2007) using an independent, theoretical model, which determined the gas mass within the Homunculus using the recent detection of H_2 to determine the density of the gas. Note that the dust mass quoted here is different to G06, since the submm flux attributed to dust emission has decreased in this work, yet the dust temperature required to fit the steeper slope between 175 μm and 1000 μm is colder here, thereby increasing the mass.

4.2 Mass Loss traced by the Submillimetre Emission

The LABoCa submm emission is interior to the X-ray shell (tracing blast wave material), the O III veil (tracing the recent N-rich mass loss interacting with older O-rich material (Smith et al. 2005) and the fast blast wave from recent ejecta interacting with the older N-rich material (Smith 2008). Since we have little information about the true structure of the submm source, the LABoCa emission is most likely a complex combination of the mass lost during the great ejection phases over the last few hundred years, and the pre-outburst stellar wind material ejected over the last few thousand years. From our constraints on the spatial location of the dust, we therefore estimate an *average* mass loss rate of $>10^{-2} M_{\odot} \text{ yr}^{-1}$, at least one order of magnitude higher than suggested in Hillier et al. (2001) and Smith et al. (2005). We are currently unable to resolve the features within the Homunculus and pin down the exact distribution or contributions of the free-free and dust components, hence our mass loss has a large associated uncertainty. We do not know the exact timescale over which the mass has been lost nor the composition and radiation properties of the dust grains. The longer timescale put on the submm mass loss in this work compared to G06, eases the strain on the available mass reservoir of η Car (Smith 2009b), since the 40 M_{\odot} of gas traced by the submm is likely a combination of eruptions and the stellar wind. However, we note that such a huge mass loss does provide support for the idea of dredge-up SN-like events and also hints that pre-SN mass loss could be significant contributors to the interstellar dust budget in the early Universe (Morgan & Edmunds 2003; Dwek, Galliano & Jones 2007).

5 CONCLUSIONS

We found that the submm extended emission surrounding η Car, originally identified in G06, is unresolved by the LABoCa beam at 870 μm , and is highly variable, following the well-documented cycle seen at mm and radio wavelengths. Accounting for the flux difference from G06 and associating the 800–1000 μm with free-free emission rather than thermal emission from grains, we revise the dust mass in the stellar wind to $0.4 \pm 0.1 M_{\odot}$. This translates to a mass loss greater than 40 M_{\odot} over the past 1000 years. Future observations with Herschel and ALMA are needed to constrain the

submm and mm variability and multi-epoch data will allow us to separate out the dust and free-free components throughout the cycle. Higher angular resolution data are needed to separate out the multiple phases of mass loss, this will provide crucial information about the evolutionary path to massive-star SN explosions.

ACKNOWLEDGEMENTS

We thank the anonymous referee for insightful comments which greatly improved this work. This publication is based on data acquired with APEX (project 078.F-9036(A) which was a joint science verification project with 078.F-9017, PI Kramer), a collaboration between the Max-Planck-Institut für Radioastronomie, the European Southern Observatory, and the Onsala Space Observatory. We thank the APEX staff for their help with observing and data analysis. We thank Nathan Smith and Kate Brooks for providing the $H\alpha$ and SIMBA maps. HLG acknowledges support from LCOGT.

REFERENCES

- Abraham Z., Falceta-Gonçalves D., Dominici T. P., Nyman L.-Å., Durouchoux P., McAuliffe F., Caproni A., Jatenco-Pereira V., 2005, *A & A*, 437, 977
- Brooks K., Garay G., Nielbock M., Smith N., Cox P., 2005, *ApJ*, 643, 436
- Cox P., 1995, *RMxAC*, Vol 2, 105
- Cox P., Mezger P.G., Sievers A., Najarro F., Bronfman L., Kreysa E., Haslam, G., 1995, *A & A*, 297, 168
- Cox P., & Bronfman, 1995, *A & A*, 299, 583
- Duncan R.A., & White S.M., 2003, *MNRAS*, 338, 425
- Dunne L., Eales S., 2001, *MNRAS*, 327, 697
- Dwek E., Galliano F., Jones A.P., 2007, *ApJ*, 662, 927
- Gomez H.L., Dunne L., Eales S.A., Edmunds M.G., 2006, *MNRAS*, 372, 1133
- Güsten R., Nyman L.-Å., Schilke P., Menten K., Cesarsky C., Booth R., 2006, *A & A*, 454, L13
- James A., Dunne L., Eales S.A., Edmunds M.G., 2002, *MNRAS*, 335, 753
- Lamers H.J.G.L.M., & Cassinelli J.P., 1999, *An Introduction to Stellar Winds*, 46, Cambridge University Press, Great Britain
- Morgan H., Edmunds M.G., 2003, *MNRAS*, 343, 427
- Morris P.W., et al., 1999, *Nature*, 402, 502
- Pittard J.M., Stevens I.R., Corcoran M.F., Ishibashi K., 1998, *MNRAS*, 299, L5
- Pastorello A., et al., 2007, *Nature*, 447, 829
- Siringo G., et al., 2009, *A & A*, 497, 945
- Rathborne J.M., Burton M.G., Brooks K.J., Cohen M., Ashley M., Storey J.W., 2002, *MNRAS*, 331, 85
- Smith N., 2008, *Nature*, 455, 201
- Smith N., 2009, available at astro-ph/0906.2204
- Smith N., Ferlund G.J., 2007, *ApJ*, 655, 911
- Smith N., Bally J., & Morse J.A., 2003, *ApJ*, 587, L105
- Smith N., Gehrz R.D., Hinz P.M., Hoffmann W.F., Hora J.L., Mamajek E.E., Meyer M.R., 2003, *ApJ*, 125, 1458
- Smith N., Morse J.A., Bally J., 2005, *AJ*, 130, 1778
- Smith N., Chornock R., Silverman J.M., Fillipenko A.V., Foley R.J., 2009, submitted to *ApJ*, available at astro-ph/0906.2200
- Teodoro M., Daminieli A., Sharp R.G., Groh J.H., Barbosa C.L., 2008, *MNRAS*, 387, 564 ASP Conference Series, Vol. 332, eds. R. Humphreys and K. Stanek, p.129
- Wright A.E., & Barlow M.J., 1975, *MNRAS*, 170, 41
- Yonekura Y., Asayama S., Kimura K., et al., 2005, *ApJ*, 634, 476